

Geometrical effects on energy transfer in disordered open quantum systems

Cite as: J. Chem. Phys. **138**, 204309 (2013); <https://doi.org/10.1063/1.4807084>

Submitted: 31 December 2012 . Accepted: 06 May 2013 . Published Online: 29 May 2013

M. Mohseni, A. Shabani, S. Lloyd, Y. Omar, and H. Rabitz



View Online



Export Citation



CrossMark

ARTICLES YOU MAY BE INTERESTED IN

[Environment-assisted quantum walks in photosynthetic energy transfer](#)

The Journal of Chemical Physics **129**, 174106 (2008); <https://doi.org/10.1063/1.3002335>

[Energy-scales convergence for optimal and robust quantum transport in photosynthetic complexes](#)

The Journal of Chemical Physics **140**, 035102 (2014); <https://doi.org/10.1063/1.4856795>

[Highly efficient energy excitation transfer in light-harvesting complexes: The fundamental role of noise-assisted transport](#)

The Journal of Chemical Physics **131**, 105106 (2009); <https://doi.org/10.1063/1.3223548>

Lock-in Amplifiers
up to 600 MHz



Zurich
Instruments



Geometrical effects on energy transfer in disordered open quantum systems

M. Mohseni,^{1,2} A. Shabani,^{3,4} S. Lloyd,⁵ Y. Omar,^{2,6} and H. Rabitz³

¹Research Laboratory of Electronics, Massachusetts Institute of Technology, Cambridge, Massachusetts 02139, USA

²Physics of Information Group, Instituto de Telecomunicações, P-1049-001 Lisbon, Portugal

³Department of Chemistry, Princeton University, Princeton, New Jersey 08544, USA

⁴Department of Chemistry, University of California, Berkeley, California 94720, USA

⁵Department of Mechanical Engineering, Massachusetts Institute of Technology, Cambridge, Massachusetts 02139, USA

⁶CEMAPRE, ISEG, Universidade Técnica de Lisboa, P-1200-781 Lisbon, Portugal

(Received 31 December 2012; accepted 6 May 2013; published online 29 May 2013)

We explore various design principles for efficient excitation energy transport in complex quantum systems. We investigate energy transfer efficiency in randomly disordered geometries consisting of up to 20 chromophores to explore spatial and spectral properties of small natural/artificial Light-Harvesting Complexes (LHC). We find significant statistical correlations among highly efficient random structures with respect to ground state properties, excitonic energy gaps, multichromophoric spatial connectivity, and path strengths. These correlations can even exist beyond the optimal regime of environment-assisted quantum transport. For random configurations embedded in spatial dimensions of 30 Å or 50 Å, we observe that the transport efficiency saturates to its maximum value if the systems contain around 7 or 14 chromophores, respectively. Remarkably, these optimum values coincide with the number of chlorophylls in the Fenna-Matthews-Olson protein complex and LHC II monomers, respectively, suggesting a potential natural optimization with respect to chromophoric density. © 2013 Author(s). All article content, except where otherwise noted, is licensed under a Creative Commons Attribution 3.0 Unported License. [<http://dx.doi.org/10.1063/1.4807084>]

I. INTRODUCTION

Monitoring and quantifying the effects of condensed phase environments on the quantum dynamics of charge and energy transfer has been one of central issues in chemical physics.^{1,2} One problem of fundamental and practical relevance is to engineer excitonic energy migration in disordered materials and nano-structures by exploiting the interplay of quantum effects and environmental interactions. This rational design approach can be influenced by recent observations of Environment-Assisted Quantum Transport (ENAQT) in biological light-harvesting systems.^{3–13} Specifically, one might develop radically novel design principles by manipulating delocalized exciton dynamics through engineering coherent couplings of free Hamiltonian and/or the environmental interactions to generate optimal efficiency. If one can fully understand the fundamental microscopic processes involved, it will be in principle possible to use *structure* for steering the ultrafast migration of excitons via quantum interference effects. Thus the excitons could be guided around defects and through interfaces in disordered systems with potentially important application in photodetection, bio-sensing, and photovoltaic systems.¹⁴

In this work, we investigate the underlying geometrical and dynamical physical principles for efficient energy transport in generic *random* multichromophoric structures typically far from symmetrized configurations considered in Refs. 15 and 16. Our work is motivated by recent studies on disorder biological light-harvesting systems,¹⁷ such as

Fenna-Matthews-Olson (FMO) of green sulfur bacteria,^{3,10} reaction center (RC) of purple bacteria,¹⁸ and light-harvesting complex II of higher plants.²⁰ In particular, we investigate generic disordered configurations of up to 20 chromophores. We examine the energy transfer efficiency of the uniformly distributed random light-harvesting complexes, as well as important subsets of these samples, encapsulated in a sphere of fixed diameter. For spatial sizes of 30 Å and 50 Å, corresponding to FMO and LHCII dimensions, we find transport efficiency increases as a function of the number of chromophores and saturates around values of 7 to 9 and 14 to 17 sites, respectively. Remarkably, the number of chlorophylls for FMO and LHCII reside in this range,¹⁹ implying a potential optimization with respect to chromophoric density.

Moreover, we compute the energy transfer efficiency (ETE) of the uniform distributions of random complexes consisting of 7 chromophores encapsulated in spherical dimension of various diameters interacting with a phononic bath. This allows us to compare our results with the performance of a well-characterized natural LHC such as the FMO complex. A similar study has been performed in Ref. 21, which concludes that the FMO geometry with such high efficiency is extremely rare. In contrast to conclusions drawn in the Ref. 21, here we find that FMO performance is not rare if one uses a more accurate dynamical model, an appropriate measure of efficiency, and limits the search space to those configurations with similar compactness level as the FMO itself. We use ETE as the yield function for performance of these random systems and use a time-convolution master equation

(TC2)²² to estimated energy transport efficiency beyond perturbative and Markovian regimes.^{11,12} We extensively explore the effect of spatial compactness on the transport efficiency and robustness due to its potential significance as recently reported in Ref. 12. Our simulations show that for larger size complexes the optimal configurations are not robust with respect to angular orientation of dipole moments in contrast to highly dense systems such as FMO.

To explore potential geometrical patterns, we examine possible spatial and energetic correlations among 10^4 random multichromophoric samples embedded in a fixed diameter sphere ranging from 30 Å to 100 Å. As we would like to explore the generic behavior of multichromophoric systems, here we do not account for spatial constraints due to any particular size and shape of the chromophores, or any specific protein or solvent environment. We also ignore the detrimental effect of concentration quenching.^{13,23} With these assumption, we find some significant statistical correlations can exist among very high- and low-efficient samples even in suboptimal regime of chromophoric density, beyond the robust ENAQT regime.¹² Specifically, we find certain structural similarities among various Frenkel exciton Hamiltonians of the high/low efficient random configurations with respect to ground state properties, excitonic energy gap structures, and spatial connections. Moreover, we introduce a new measure of spatial *path strength* that can quantify an underlying structural mechanism for the performance of light-harvesting systems in a given dimension.

This paper is organized as follows: In Sec. II, we describe our physical model and review the non-local master equation that was derived and analyzed in Ref. 11 to efficiently calculate ETE in multichromophoric systems. In Sec. III, we examine the variation of ETE with the number of chromophores in fixed dimensions. In Sec. IV, we explore the role of chromophoric density in energy transfer as a dominating parameter.¹² In the subsequent sections we explore the roles of other physical parameters in transport including, ground state energy properties, average excitonic energy, structure and strength of chromophoric connectivity.

II. THEORETICAL MODEL OF RANDOM MULTICHROMOPHORIC SYSTEMS

Based on the generalized Bloch-Redfield master equations introduced by Cao,²⁴ we have recently derived the well-known time nonlocal master equation TC2 without making the usual weak system-bath coupling assumption.¹¹ By providing an error analysis, we could show that TC2 can be employed for highly efficient while reliable estimation of energy transfer efficiency in light-harvesting complexes for both weak and intermediate system-bath coupling strengths and memory time scales. Here, we summarize the main steps of our approach. More technical details can be found in Ref. 11.

The dynamics of a photosynthetic system interacting with the surrounding scaffold protein and solvent can be understood by starting from a general time evolution formulation of open quantum systems. The total system-bath

Hamiltonian can be expressed as

$$H_{total} = H_S + H_{ph} + H_{S-ph}, \quad (1)$$

where

$$H_S = \sum_{j,k} \epsilon_j |j\rangle \langle j| + J_{jk} |j\rangle \langle k|,$$

$$H_{ph} = \sum_{j,\xi} \hbar \omega_\xi (p_{j,\xi}^2 + q_{j,\xi}^2)/2,$$

$$H_{S-ph} = \sum_j S_j B_j.$$

The phonon bath is modeled as a set of harmonic oscillators. Here $|j\rangle$ denotes an excitation state in a chromophore spatially located at site j . The diagonal site energies are denoted by ϵ_j s that include reorganization energy shifts $\lambda_j = \sum_\xi \hbar \omega_\xi d_{j,\xi}^2/2$ due to interactions with a phonon bath; $d_{j,\xi}$ is the dimensionless displacement of the (j, ξ) th phonon mode from its equilibrium configuration. The strengths of dipole-dipole interactions between chromophores in different sites are represented by J_{jk} . The operators $S_i = |i\rangle \langle i|$ and $B_j = -\sum_\xi \hbar \omega_\xi d_{j,\xi} q_{j,\xi}$ are system and bath operators. Here, we assume that each site is linearly interacting with a separate phonon bath. The overall dynamics of the system is given by Liouvillian equation,

$$\frac{\partial \rho_S(t)}{\partial t} = -i \hbar \langle [H_{total}, \rho_{SB}(t)] \rangle_{ph} = \langle \mathcal{L}_{total}[\rho_{SB}(t)] \rangle_{ph}, \quad (2)$$

where ρ_{SB} denotes the system-bath state, and $\langle \dots \rangle_{ph}$ indicates an average over phonon bath degrees of freedom. The Liouvillian superoperator \mathcal{L}_{total} is the sum of superoperators \mathcal{L}_S , \mathcal{L}_{ph} , and \mathcal{L}_{S-ph} associated to H_S , H_{ph} , and H_{S-ph} , respectively. The time evolved density operator of the multichromophoric systems in the interaction picture can be expressed by the propagator,

$$\tilde{\rho}(t) = \left\langle \mathcal{T}_+ \exp \left[\int_0^t \tilde{\mathcal{L}}_{total}(s) ds \right] \right\rangle_{ph} \rho(0), \quad (3)$$

where \tilde{O} denotes the interaction picture representation for an operator O . If we expand the above time-ordered exponential function, we arrive at the Dyson expansion for time evolution of the density operator. This expansion involves multi-time bath correlation functions $\langle \tilde{B}(t_{i_1}) \dots \tilde{B}(t_{i_n}) \rangle_{ph}$, for any $B = B_j$. According to generalized Wick's theorem, for a system interacting with a bosonic (photonic and/or phononic) bath these higher order bath correlation functions can be exactly described by various combinations of only two-time correlation functions of the form $\prod_{l,k} \langle \mathcal{I}_+ \tilde{B}(t_{i_l}) \tilde{B}(t_{i_k}) \rangle$, where \mathcal{I}_+ is the index ordering operator. Assuming such Gaussian property for bath fluctuations, the most general approach to solve the master equation (2) is to utilize a path integral formalism, leading to HEOM.²⁵ However, such general approach is impractical for our purpose as the computational resources required for simulating the energy transfer dynamics of photosynthetic complexes grow significantly with increasing size of the system, and with decreasing bath cutoff frequency and ambient temperature.

We derived a numerically efficient method for simulation of complex excitonic systems by incorporating some physical approximations in addition to the Gaussian property to map

quantum dynamics into a single solvable time-nonlocal equation, see Ref. 11. The main approximation is involved with a special truncation of higher-order bath correlation functions. Specifically, we assumed that the generalized Wick's expansion

$$\langle \tilde{B}(t_{i_1}) \dots \tilde{B}(t_{i_{2n}}) \rangle_{ph} = \sum_{pairs} \prod_{l,k} \langle \mathcal{I}_+ \tilde{B}(t_{i_k}) \tilde{B}(t_{i_l}) \rangle, \quad (4)$$

can be approximated as

$$\langle \tilde{B}(t_{i_1}) \dots \tilde{B}(t_{i_{2n}}) \rangle \approx \langle \mathcal{I}_+ \tilde{B}(t_1) \tilde{B}(t_2) \rangle \langle \mathcal{I}_+ \tilde{B}(t_{k_3}) \dots \tilde{B}(t_{k_{2n}}) \rangle \quad (5)$$

for $t_1 > t_2 > \dots > t_{2n}$. In other words, we disregard some fast decaying terms in the generalized Wick's expansion, but keep the slow decaying leading terms such that a two-point correlation can be factored out. This approximation can be understood phenomenologically by noting that two-point correlation functions $C_j(t - t_1) = \langle \tilde{B}_j(t) \tilde{B}_j(t_1) \rangle$ typically decay over a characteristic time, e.g., for a Lorentzian spectral density and at high temperature T , the correlation functions decay exponentially as $\lambda(2/\beta - i\gamma)e^{-\gamma(t-t_1)}$ where γ^{-1} is the relaxation time of phonons and $\beta = (k_B T)^{-1} < \gamma^{-1}$. The approximation (5) is valid in the limit of time scales t longer than γ^{-1} . As we see below, in calculating ETE we are considering an integration over time therefore this approximation can provide good results even if γ is not large or in another word we are in a relatively non-Markovian regime.

Using this approximation we arrive at the time non-local master equation, TC2, as

$$\begin{aligned} \frac{\partial}{\partial t} \rho(t) = & \mathcal{L}_S \rho(t) + \mathcal{L}_{e-h} \rho(t) \\ & - \sum_j \left[S_j, \frac{1}{\hbar^2} \int_0^t C_j(t-t') e^{\mathcal{L}_S(t-t')} \right. \\ & \left. \times S_j \rho(t') dt' - h.c. \right], \end{aligned} \quad (6)$$

where $\mathcal{L}_{e-h} = -\sum_j r_{loss}^j \{ |j\rangle \langle j|, . \} - r_{trap} \{ |trap\rangle \langle trap|, . \}$, $h.c.$ stands for Hermitian conjugate, and $\{.,.\}$ is the anti-commutator ($[.,.]$ is the commutator). The vector $|trap\rangle$ denotes the state of the site (bacteriochlorophyll (BChl)) connected to the reaction center. The term $\mathcal{L}_{e-h} = -\sum_j r_{loss}^j \{ |j\rangle \langle j|, . \} - r_{trap} \{ |trap\rangle \langle trap|, . \}$ captures two different competing electron-hole pair recombination processes that determine the energy transfer efficiency of light harvesting complexes. The first process, *loss*, is due to dissipation to the environment at each site that happens within the time scale of 1 ns. This adverse environmental effect guarantees that the energy transfer efficiency has a value less than one. The second recombination process, *trap*, is due to successful trapping at one or more reaction center(s).

A biologically relevant function for exploring the performance of light-harvesting complexes is ETE as defined in Refs. 4, 26, and 27, that is the total probability of exciton being successfully trapped,

$$\eta = 2r_{trap} \int_0^\infty \langle trap | \rho(t) | trap \rangle dt. \quad (7)$$

We provide a formal derivation of the energy transfer efficiency in Ref. 11. ETE measures the likelihood of successful trapping, weighted by trapping rate: it quantifies the excitation availability whenever the reaction center is ready to operate within a period much shorter than the exciton life-time.²⁶ Note that this definition is very different than the first passage time measure,^{21,28} which quantifies the time scale of the first arrival of an exciton to the trapping sites. The latter definition is not necessarily correlated with the efficiency of quantum transport. In other words, for certain quantum processes the first passage time can be very short, compare to all other time scales, but the transport mechanism could be still inefficient. In such cases, the excitations are typically delocalized over the regions that have very small overlaps with the reaction center and thus dissipate into the environment.

The primary motivation for the truncation of correlation functions introduced above is to obtain a special time non-local master equation that is solvable in the frequency domain. To estimate the regimes of the applicability of this method, one would ideally need to account quantitatively for the errors introduced by the generalized Wick's expansion truncation (5). We presented an approximate estimation of such inaccuracy in Ref. 11 for computing energy transfer efficiency by defining an upper bound for the error as

$$\Delta\eta = 2r_{trap} \left| \int_0^\infty \langle trap | \rho(t) - \rho_{TC2}(t) | trap \rangle dt \right|, \quad (8)$$

where $\rho(t)$ is the exact density matrix of the system and $\rho_{TC2}(t)$ is the solution to the TC2 master equation. Note that an exact account of errors in various regimes of interest is equivalent to calculating the general evolution of the density operator of the system that we intend to avoid. In Ref. 11, using a combination of phenomenological and analytical approaches, we found an approximate error bound for weak and intermediate system-bath couplings and bath memory time scales, thus quantifying the reliability of our approach in such regimes. We also tested the accuracy of our method by examining its predication in simulating quantum dynamics of FMO complex at room temperature compare to HEOM as a general benchmark.²⁹ We showed that oscillatory time evolution of the population of BChls in the FMO using our approach is relatively close to those predicted by HEOM.¹¹ Here we should emphasize that although Eq. (6) can be applied for any bath correlation function, but our error analysis in Ref. 11 is limited to an exponentially decaying function $C_j(t - t_1)$ corresponding to a Drude-Lorentz bath spectral density. The same limitation holds in our comparison between TC2 and HEOM, as HEOM applied in Ref. 29 considers a Drude-Lorentzian spectral density.

Here, we would like to apply TC2 master equation to explore the interplay of structurally-induced quantum coherence and environmental interactions for a large number of small-size random light-harvesting complexes with different chromophoric densities. We choose the magnitudes of dipole moments similar to FMO, but with arbitrary random orientations, site energies, and locations bounded in any given diameter of the spherical space. Our results hold for other materials with different dipole moment magnitudes by an appropriate renormalization of distances in spherical coordinate. We set

the nearest neighbor distances by a lower bound of 5 \AA due to intrinsic limitation of the dipole-dipole approximation.³⁰ Since we are interested in the generic behavior of multichromophoric systems, our model has no inclusion of spatial constraints due to particular size or shape of chromophores or the environment structure, being either the scaffold protein or the solvent. We assume that the initial excitation and trapping sites are located at the surface of the sphere encapsulating a given configuration. That enables us to avoid a large amount of trivial optimal solutions in the configuration spaces; i.e., those in which the original donor and final acceptor sites are nearest neighbors. Thus the exciton has to travel through the entire length of the multichromophoric complex and generally experiences multi-path quantum interference in the regime of interest with intermediate system-bath coupling strength.

III. OPTIMAL NUMBER OF CHROMOPHORES

Here, we explore the dependency of ETE on the number of chromophores for small light-harvesting complexes. In Fig. 1, we plot ETE for random complexes consist of 2 to 20 chromophores embedded in spheres of diameter $d = 30 \text{ \AA}$, and $d = 50 \text{ \AA}$ with environmental parameters given in Ref. 31. The average ETE for 1000 random configurations is computed for fixed diameters and fixed number of chromophores. The standard deviation in these samples is depicted in the inset of Fig. 1. We observe that ETE increases monotonically by increasing the number of chromophores for different compactness levels. It is remarkable that for $d = 30$, which is the same as the diameter of the FMO complex, the range seven to nine represents the minimal set of chromophores necessary to obtain high efficiency of 98%. Although, slightly higher ETE can be obtained by additional sites, that would be practically inefficient considering the amount of work required to form such extremely dense multichromophoric system for a marginal improvement in ETE. Here, the minimalist nature of natural selection might be at work: complexity is added until high efficiency and robustness is attained. A similar behavior can be seen for $d = 50$ which coincides with

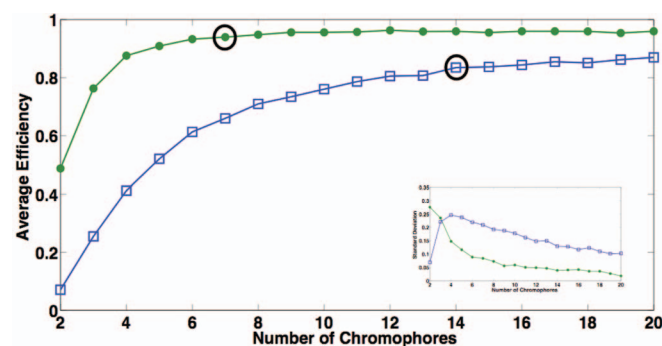


FIG. 1. The average energy transfer efficiency of random configurations consisting of different numbers of chromophores. The green [blue] dots represent the average ETE for 10^3 random multichromophoric complexes embedded in a sphere of diameter 30 \AA [50 \AA]. The ETE increases with the number of sites saturating around 7 to 9 and 14 to 17 which, respectively, coincide with the number of chromophores in the FMO and LHCII monomers with spatial dimensions of 28.5 \AA and 47 \AA . These results imply a potential optimization of chromophoric density in nature.

the spatial size of LHCII. In such a distance, the ETE also saturates by increasing the number of sites and reaches to its optimal range of about 14 to 17 chromophores. Any extra chromophore may improve the average efficiency by less than 1%. Ironically, 14 is the number of chromophores of the LHCII monomers in higher plants.

We expect that such saturation of ETE with respect to the number of chromophores to occur for other range of compactness levels. It is of great importance if similar comparisons with larger natural photosynthetic complexes can be demonstrated. That would imply a potential natural optimization with respect to the number of chromophores participating in quantum transport. Similar studies for larger artificial light-harvesting complexes could be of significant value for estimating the minimal number of chromophores needed to achieve a desired efficiency considering the physical and chemical spatial constraints in a realistic environmental condition. Such studies are beyond the scope of the current paper and will be undertaken in subsequent works. Next, we explore the role of chromophoric density by considering a fixed number of dipoles in various spatial dimension.

IV. FUNDAMENTAL ROLE OF CHROMOPHORIC DENSITY

We investigate the efficiency of random light-harvesting complexes, sampled from uniform distributions, embedded in a sphere of given diameter, d , ranging from 30 \AA to 100 \AA . For each compactness level defined by a fixed diameter, we categorize the population of 10^4 random arrangements in various classes based on their respective ETE and reorganization energies. Figure 2 shows the histograms of such populations for various multichromophoric diameters for three different values of reorganization energy chosen from the three different regions of system-bath couplings strength including intermediate regime, e.g., $\lambda = 35 \text{ cm}^{-1}$ (green bars), fully coherent regime with virtually no environment 0 cm^{-1} (blue bars), and strong environmental interactions, e.g., 350 cm^{-1} (red bars).

Let us first examine the results associated to those complexes living in the similar environment as FMO (green bars in Fig. 2). Observe that an overwhelming amount of random configurations have efficiencies comparable to the FMO complex for compactness level of about $d = 30 \text{ \AA}$. Thus, in contrast to conclusions drawn in the Ref. 21, the FMO performance is not rare if one limits the parameter space to those configurations that have a similar compactness as the FMO protein complex. Also, here we are using ETE as a measure of performance which captures long-time behavior on the same order as trapping time scale. In addition, we use a TC2 dynamical equations that can go beyond Haken-Strobel model and captures relaxations as well as pure dephasing process.

Our results in Fig. 2 introduce an additional degree of the robustness for the FMO complex. It implies excellent tolerance with respect to the BChls locations, provided that its boundaries and environment are not changing radically. This robustness is different than relative insensitivity of FMO transport efficiency to dipole orientations and site energies that were reported by us in Ref. 12. Notably, as we increase the size of random complexes from 30 \AA to 100 \AA ,

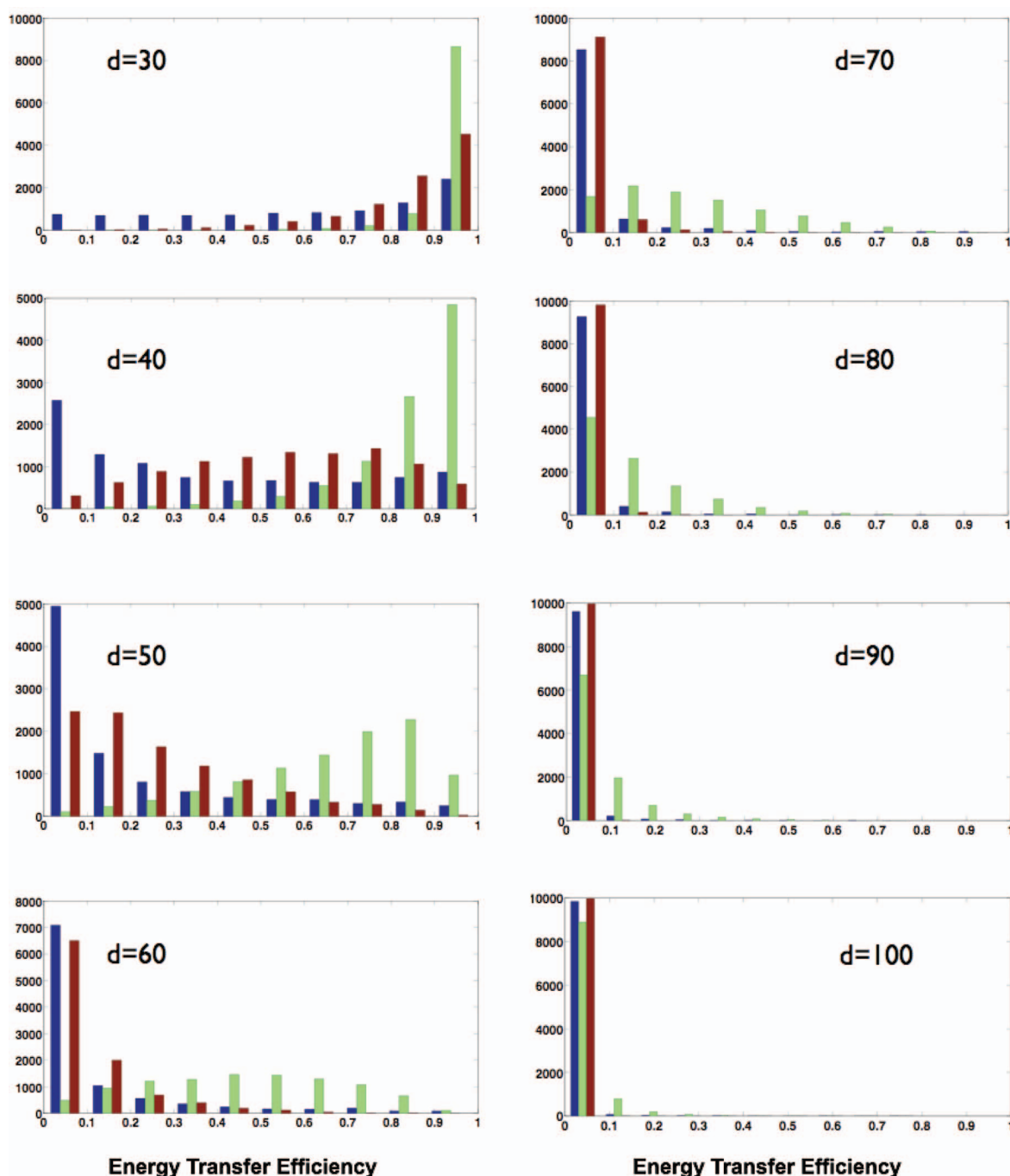


FIG. 2. The effect of chromophoric compactness on ETE for different system-bath coupling strength. We simulate ETE for 10^4 different configurations of 7 chromophores embedded in a sphere of fixed diameter d ranging from 30 Å to 100 Å. The initial and target chromophores are located on the north and south poles of the spheres. The ETE histogram is depicted for reorganization energies of $\lambda = 0 \text{ cm}^{-1}$ (blue), $\lambda = 35 \text{ cm}^{-1}$ (green), and $\lambda = 350 \text{ cm}^{-1}$ (red). At $\lambda = 35 \text{ cm}^{-1}$ and $d = 60$ a uniform distribution in all classes of ETE is observed. Below $d = 60$ the samples are mostly high efficient and above $d = 60$ they become mostly low efficient. For $\lambda = 0$ and 350, this transition happens around $d = 40$ indicating that optimality and robustness of ETE can both be enhanced by the appropriate level of environmental fluctuations. The FMO complex belongs to an ultrahigh performing population represented by green bars in $d = 30$ implying the highest degree of efficiency and fault-tolerance in such chromophoric density and noise level.

for fixed $\lambda = 35 \text{ cm}^{-1}$ (green bars), the histograms are drastically changing from being sharply peaked at high ETE to have sharp spectrum at low ETE, with average ETE dropping monotonically from 94% in $d = 30 \text{ Å}$ to 3% in $d = 100 \text{ Å}$. In the intermediate sizes, $d = 50 \text{ Å}$ to $d = 70 \text{ Å}$, we observe that these samples are more or less evenly distributed in all efficiency levels with mean value of about 50 % efficiency for

$d = 60 \text{ Å}$. This implies a smooth transition in ETE standard deviation, as a function of an effective parameter μ^2/d^3 , with optimal values around $d = 60 \text{ Å}$.

One might expect that simple geometrical patterns can fully describe the variations of ETE in a given spatial dimension. For example, it is intuitively expected that straight line arrangements of the chromophores from the initial excitation

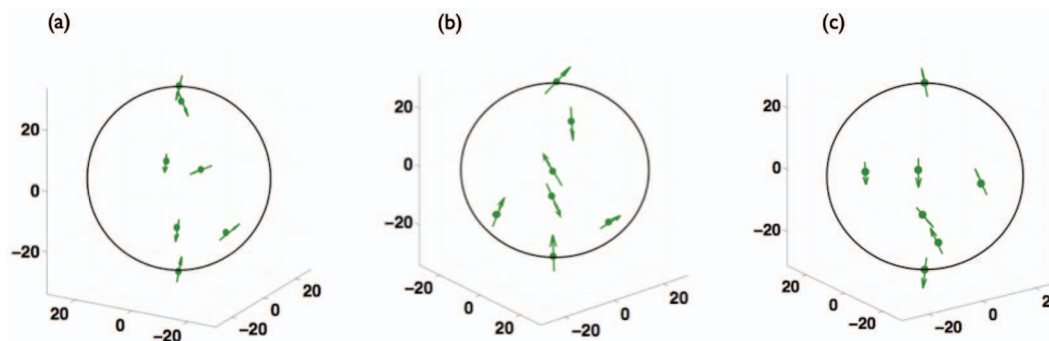


FIG. 3. Three samples of chromophoric arrangements from the 10^4 random configuration in Fig. 2 for $d = 60$ Å and $\lambda = 35$ cm $^{-1}$. These samples have distinct energy transfer efficiencies including very low efficiency of less than 1% in (a), intermediate efficiency of about 50% in (b), and high efficiency of around 93% in (c). It can be observed that simple geometrical considerations of spatial coordinates of chromophoric dipole moments cannot fully account for the significant discrepancies in their efficiencies.

to the trapping site should lead to more efficient configurations in a fixed dimension. However, by inspection of the actual locations of the chromophores for three random samples associated to diameter of $d = 60$ Å we note that these apparently similar samples have significantly different energy transfer efficiencies, see Fig. 3. Thus, other structural and dynamical correlations should play important roles in discriminating among various samples with respect to ETE. We consider a variety of possible scenarios in the following sections. One potential important factor is the effect of environmental interactions on the shape of the ETE histograms and its transition from mostly efficient to mostly inefficient regimes.

To study the impact of ENAQT on the above phenomenon, we simulate ETE for random chromophoric configurations in two extreme environmental cases in Fig. 2. Blue bars represent the ETE for the ideal case of isolated systems and red bars show ETE for the systems that are strongly interacting with their surroundings (e.g., one order of magnitude stronger reorganization energies). The general features of the ETE histogram persist but transitions occur in smaller dimensions for both of these cases around $d = 35$ Å to $d = 45$ Å. Thus the existence of ETE statistical transition is independent of ENAQT. This phenomenon is essentially a direct manifestation of quantum dynamics driven by the internal Hamiltonian, but its effect is modulated by reorganization energy. The ENAQT phenomenon can be seen here by noting that

those configurations operating at ($\lambda = 35$ cm $^{-1}$), represented by green bars, always have higher ETE at all compactness levels.

Overall, by careful inspection of these results two main questions arise: How does the ETE behave as a function of the chromophoric density? What are the possible classical and/or quantum correlations, in the spatial and energetic structure of these random multichromophoric geometries, discriminating ultrahigh or ultralow efficiencies in any fixed diameter? We addressed the former question in details in the Ref. 12 by examining the variation of the average transport efficiency for random configurations of up to 20 chromophores in two different compactness level. We observed that the chromophoric density of the FMO complex and LHCI to be around the optimal values for spatial dimensions of $d = 30$ Å and $d = 50$ Å, respectively. Here, we investigate the latter question.

In Secs. V–VIII, we explore underlying structural and physical principle(s) for very high- or low-efficient 7-chromophore configurations in any of the histograms in Fig. 2, beyond the dominating factor of compactness. In the first step of our analysis of Fig. 2, we compute the average ETE over all random samples in various spatial dimensions to emphasize that very weak or strong environments are sub-optimal in all ranges, see Fig. 4(a). In Fig. 4(b) the standard deviation of the average ETE is plotted for the same compactness levels highlighting the diversity of configurations with a

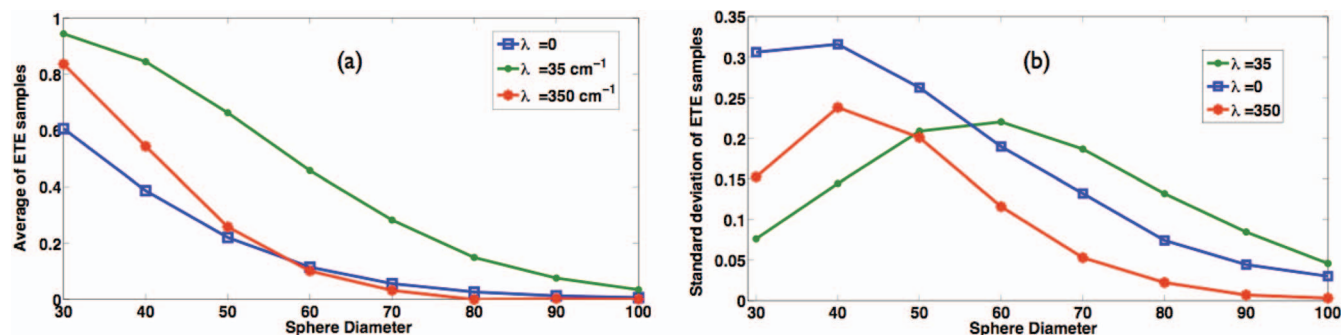


FIG. 4. The average (a) and the standard deviation (b) of ETE in the samples given in Fig. 2. The average ETE drops monotonically by increasing the diameter of the sphere from $d = 30$ Å to $d = 100$ Å. The standard deviation shows a maximum around $d = 60$ Å (40) for $\lambda = 35$ cm $^{-1}$ (0 or 350). In such compactness regimes, the diverse populations of random configurations from very low to very high efficiency implies lack of robustness due to significant involvement of other physical parameters in guiding the exciton migration ETE, beyond the dominating factor of chromophoric density.

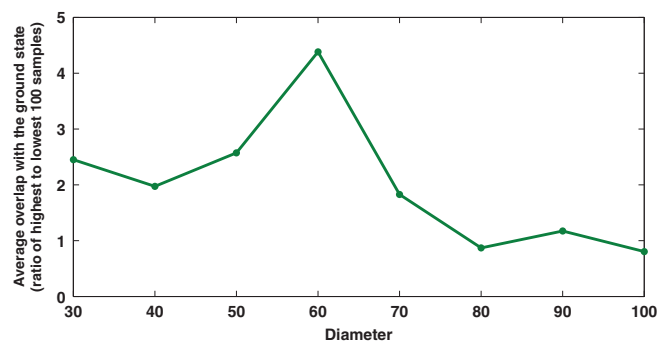


FIG. 5. The overlap between the Hamiltonian ground state and the trapping site 3 is presented for the ratio of the average top 100 efficient random samples over bottom 100 configurations. Although high efficiency geometries have larger overlap, especially at dimension $d = 60$ Å, the overlap of ground at trapping site cannot fully account for the large discrepancies among top 100 efficient and 100 low efficient configurations.

maximum pick at the range $d = 40$ to $d = 60$ Å for different reorganization energy values.

V. GROUND STATE ENERGY OVERLAPS

Based on the definition of ETE, one generally expects that the overlap of lowest exciton state (ground state) with the trapping site to be a good indicator of any potential correlations among highly efficient samples. This overlap is indeed very high for the FMO complex, about 0.94. In order to test this hypothesis, we have diagonalized the free Hamiltonian of the top 100 high efficiency and bottom 100 low efficiency random samples, and calculated the average overlap between ground excitonic state with trapping. Figure 5 shows the ratio of such average overlaps for highest 100 samples to lowest 100 samples. We note that some global correlations exist as the ground state overlap is bigger by a factor as high as 4.5 for the high efficient samples in most compactness levels with maximum enhancement around $d = 60$ Å. However, this correlation is incomplete, since it cannot account for huge discrepancies in ETE within each distribution. In particular, this measure cannot accurately discriminate ultrahigh (low) efficient samples (top/low 10 configurations) from the rest of geometries. Moreover, it cannot directly account for the role of environment.

VI. EXCITONIC-PHONONIC ENERGY CONVERGENCE

One measure that can potentially capture the role of environment in discriminating among various configurations is the compatibility of exciton energy gaps with phonon energies. In the weak system-bath couplings the multiphonon transitions are not common and most of environment induced dynamics is driven by single phonon transitions. In such regimes, those configurations that have exciton energy gaps comparable with the energies of phonons can easily use the bath as an energy sink. This can lead to enhancement of funneling toward trapping sites by passing extra energy to phonons in a fixed excitation manifold. Using bosonic distribution function, a rough estimation of the average energy of a phonon can be simply

evaluated by ignoring the protein chemical energy as follows:

$$\frac{\int_0^\infty d\omega J(\omega)\omega/(\exp(\beta\omega) - 1)}{\int_0^\infty d\omega J(\omega)/(\exp(\beta\omega) - 1)}, \quad (9)$$

where $J(\omega)$ is the Lorentzian spectral density. Using the above relation the average energy of a single phonon is about 64 cm^{-1} , assuming bath with cutoff frequency of 50 cm^{-1} at room temperature. We also compute the average energy gaps, g , for the bottom 100 and top 100 efficiency samples. The distribution of such samples based on their average exciton gaps in various compactness levels is shown in Fig. 6. We observe that bottom 100 samples (gray bars) have average energy gaps between 200 and 400 cm^{-1} with large standard deviation of about 200 cm^{-1} , see Fig. 7. Thus, there is typically an energy mismatch between typical exciton gaps and phonon energies. On the contrary, the top 100 efficient samples have energy gaps of about 100 cm^{-1} with smaller standard deviation of about 50 cm^{-1} . Consequently, there is a considerable chance of system-bath energy exchange facilitating exciton transfer. A more accurate description of the exciton bandgap correlations should include multiphonon transitions for strong system-bath couplings that can be captured in Förster theory,³² or modified Redfield theory³³ However, our data suggest that one- or two-phonon transitions that are relevant in the intermediate regimes can be captured by our dynamical equation (6). Very recently, the relevance of matching exciton energy differences to vibrational modes energies has been reported.^{34–36}

VII. SPATIAL CONNECTIVITY

In the classical regime of incoherent hopping, a simple design principle for the multichromophoric systems, coupled via dipole-dipole interactions, to achieve high ETE would be to align chromophores on a straight line connecting the initial and target sites. In Fig. 3, we observe that relatively similar patterns might lead to configurations with very different ETE. By enlarging the spherical size encapsulating the samples, the average inter-chromophoric couplings become weaker, therefore the quantum coherence would be attenuated. Thus, we expect that the measure of proximity to the axis connecting the initial and target chromophores, z , takes lower (higher) values for high (low) efficiency samples. To this end, we examine this measure defined as the average distance of the 5 intermediating chromophores from the Z axis. This numerical study, plotted in Fig. 8, confirms such intuition to some extent. The average distance of total number of random configurations from the Z axis is plotted, as well as such distances for top 100 (high-efficient) and bottom 100 (low-efficient) samples. It can be seen that the average distances for these different classes become more distinct by increasing the dimension of the sphere. For diameter 100 Å, the top 100 samples on average are closer to Z axis compared to the total populations with a ratio of 0.6. On the other hand, this feature is less important for more compact structures and for low-efficient configurations suggesting that simple geometrical consideration per se cannot fully determine the performance of an excitonic energy transfer system.

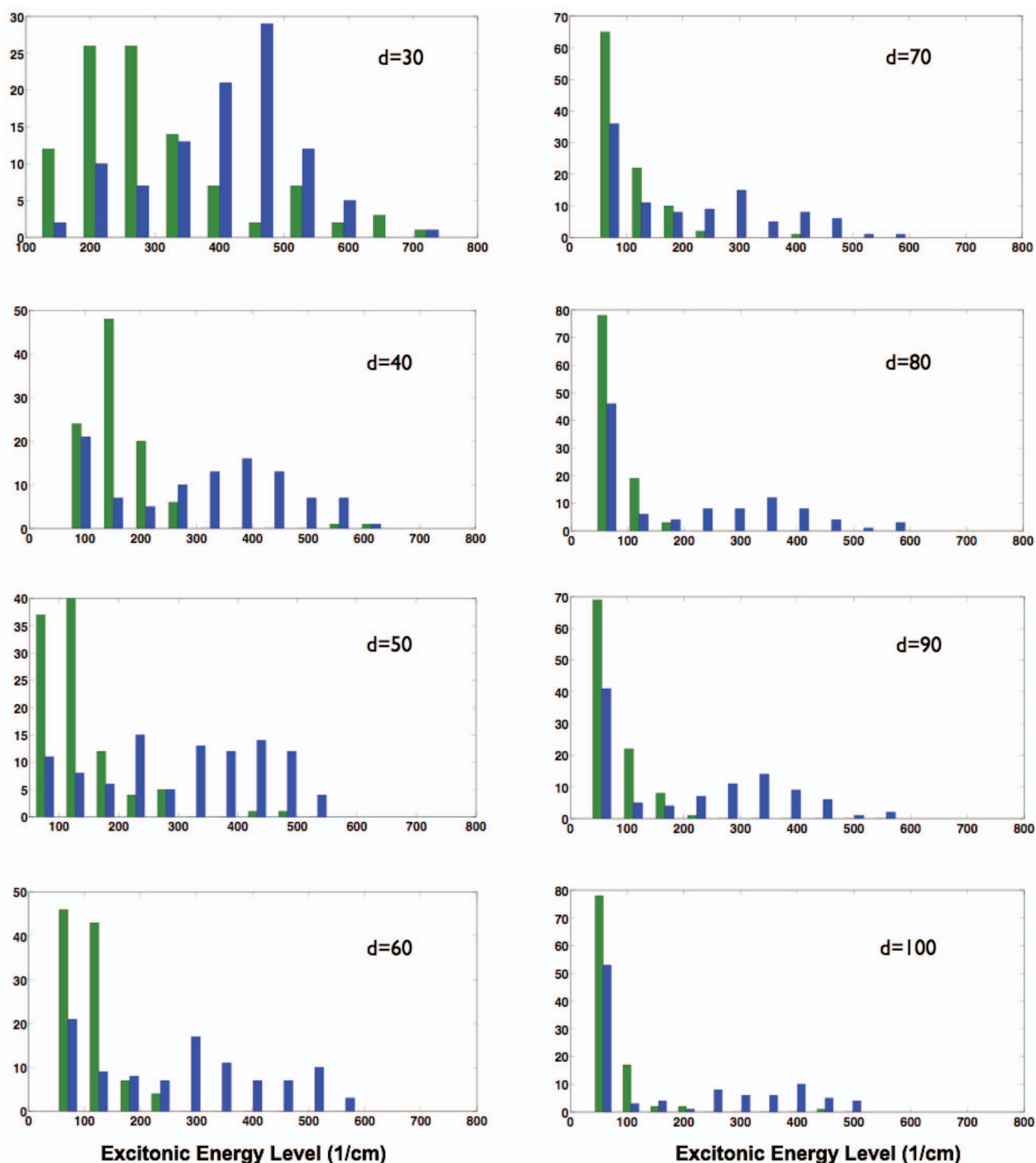


FIG. 6. The histogram of excitonic energy levels for 100 efficient samples and 100 lowest samples chosen from all 10^4 configurations embedded in spheres with different fixed diameters ranging from $d = 30$ Å to $d = 100$ Å in Fig. 2. It can be observed that for the entire range of spatial dimensions low efficiency samples have energy gaps significantly larger than the phonons average energy 63 cm^{-1} , and thus cannot use the bath as a energy sink to enhance exciton funneling in a fixed excitation limit. On the contrary, for top 100 highly efficient samples, we see that their average energy gap is sharply picked around 100 cm^{-1} or less for dimensions larger than $d = 40$ Å. We note that for $d = 30$ Å there is significant insensitivity with respect to these energy mismatches.

VIII. PATH STRENGTHS

One important structural feature of light harvesting complexes is the spatial connectivity of their constituent chromophores. Here we demonstrate that such geometrical parameters in the site base could provide an underlying physical explanation for the vast diversity of high or low energy transfer efficiency of random configurations embedded in a fixed vol-

ume, Fig. 2. We first define the concept of spatial path and its *path strength* between initial and trapping sites.

Generally, for any m -chromophoric system, there are $\sum_{k=0}^{m-2} \frac{(m-2)!}{(m-k-2)!}$ spatial paths each including different coupling combinations of $0 \leq k \leq m - 2$ chromophores connecting initial and target sites. Label the initial site as 1 and the target site as 7. A path defined by interconnecting chromophores

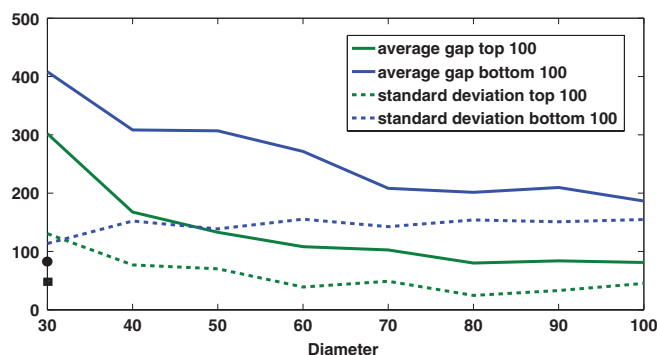


FIG. 7. The excitonic energy levels of high- and low-efficient samples. The green (blue) line shows the average energy levels of top (bottom) 100 samples. The green (blue) dashed-line shows the energy levels standard deviation of top (bottom) 100 samples. The energy of phonons at $T = 298^\circ\text{K}$ and $\gamma = 50 \text{ cm}^{-1}$ has an average of 64 cm^{-1} . It can be seen that the high-efficiency samples have energy levels in the range of phonon energies, therefore facilitating energy exchange with the bath and enhancing the ENAQT process.

$\{c_1, \dots, c_k | 1 < c_j < 7\}$, has path strength, h_{c_1, \dots, c_k} , defined as the inverse of the total time scale of going through the path from the chromophore 1 to 7. This time scale h_{c_1, \dots, c_k}^{-1} is given by the sum of the inverse of coupling strengths between neighboring sites given by the off-diagonal elements of the Hamiltonian H

$$h_{c_1, \dots, c_k}^{-1} = |H_{1, c_1}|^{-1} + \sum_{j=1}^{k-1} |H_{c_j, c_{j+1}}|^{-1} + |H_{c_k, 7}|^{-1} \quad (10)$$

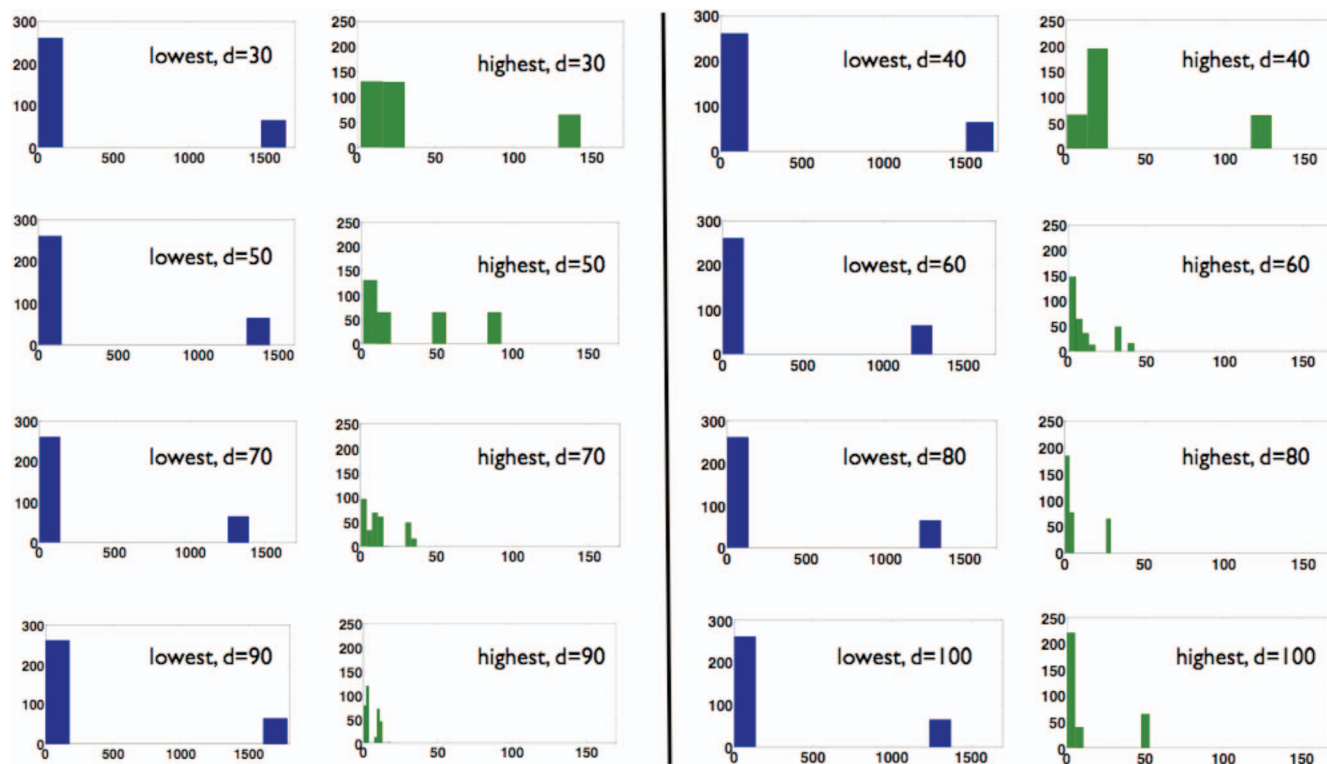


FIG. 9. The histogram of the strength of 326 possible paths connecting initial and trapping states for the very top-/low-efficiency configuration (chosen from 10^4 random 7-chromophoric light-harvesting complexes in a fixed diameter 30 \AA to 100 \AA presented in Fig. 2). In each fixed d the right (left) histogram demonstrates the number of paths for a given range of path strength, in energy units of cm^{-1} , for the most (least) efficient sample. A considerable energy gap of about 1500 cm^{-1} in the left panel is observed that is one order of magnitude bigger than those in the right panel for all volumes. There are a few strong paths that dominate the energy transport in the low efficient samples. In contrast, a large number of paths are contributing to quantum transport for high performing samples in the right panel. These alternative paths could help avoiding quantum localization due to static or dynamical disorders leading to a substantial enhancement of energy transport efficiency.

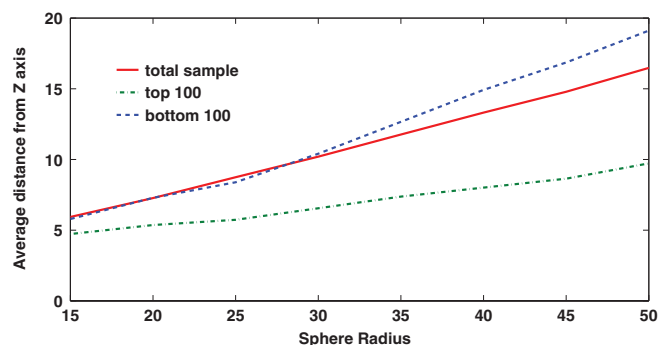


FIG. 8. The average distance of the five intermediating chromophores from the Z axis connecting the initial and target chromophores for total number of random configurations as well as top/bottom high/low efficient samples. The average distances for various ETE classes become more distinct by increasing the radius of the spheres. For larger spheres, the attenuation of quantum effects enforces the high ETE configurations to have narrower structures of intermediating chromophores. The average distance of 9.8 \AA for 100 high-efficient samples at radius 50 \AA versus 17 \AA for the total samples indicates this fact. This behavior is not significant for more compact geometries or low efficient samples.

and the trivial path of sites 1 and 7 direct connection has strength $H_{1,7}$. For a light harvesting complex consisting of 7 chromophores, there are 326 spatial paths each including a different coupling combination of one to five chromophores. In order to study any potential relationship between the path strength (as defined above) and ETE, we compute the strength

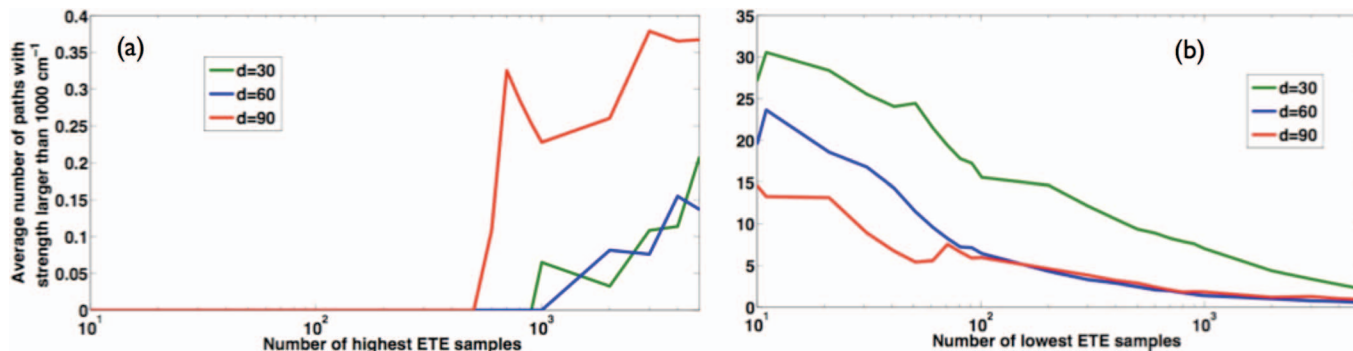


FIG. 10. (a) The number of pathways with path strength larger than 1000 cm^{-1} statistically averaged over m highest ETE samples. The horizontal axis shows the number of high ETE samples included in the statistical computation. It can be observed that top 500 high efficient configurations have no dominant pathways. If we enlarge the number of configurations beyond top 500, i.e., including samples with intermediate ETE, a few paths with strong strength will appear. (b) The number of spatial pathways with strength larger than 1000 cm^{-1} statistically averaged over m lowest ETE samples. The horizontal axis shows the number of low ETE samples contributed to the statistical average. In sharp contrast to histogram (a), the energy transfer in the low efficient configurations is dominated by a few channels with very strong path strength. This property is attenuated when we increase the number of statistical samples to include more efficient ETE configurations. These results demonstrate that the path strength, defined by Eq. (10), is a suitable measure for quantifying the geometrical mechanism for the performance of light-harvesting systems in a given spatial dimension.

for all the paths for the most and least efficient configurations, from 10 000 random 7-chromophoric samples in a given sphere with diameter 30 \AA to 100 \AA . The results are demonstrated in Fig. 9, where in each fixed d the right (left) histogram demonstrates the number of paths for a given range of strength in energy unite, cm^{-1} , for the most (least) efficient configuration.

We note that there are significant path strength gaps of about 1500 cm^{-1} in the left panel (ultralow ETE samples) which are one order of magnitude bigger than those in the right panel (ultrahigh ETE samples with gaps of less than 150 cm^{-1}) at all compactness levels. Incidentally, for low efficiency random configurations there are a few paths that completely dominate the energy transport whereas the high efficient samples contain a large number of, more or less, uniformly distributed spatial paths that contribute to quantum transport. One reasonable explanation is that light harvesting complexes with a few effective paths for exciton transport are more susceptible to large energy mismatches due to static or dynamical disorders leading to quantum localization. By contrast, those complexes with a large number of active spatial path become more robust to disorders or defects by providing alternative routes of transport. Moreover, the multi-path systems can better exploit the environmental fluctuations to overcome energy mismatches which otherwise lead to exciton localizations. A similar robustness to defects due to redundant paths has been recently observed experimentally for energy transfer in certain artificial light-harvesting complexes^{37,38} and numerically simulated using an incoherent Förster model. These artificial systems are synthesized from self assembly of tobacco mosaic virus scaffold protein in disc and rod geometries which in the latter up to thousands of chromophores can be positioned spirally. Overall, the concept of path strength provides a rather straight forward explanation for the diversity of configurations in the ETE histograms presented in Fig. 2.

To investigate this phenomenon beyond the highest or lowest efficient configurations, we have performed statistical studies on different ensembles of the samples, see Fig.

9. We observe that for the low efficient configurations the excitonic energy is carried through a few dominant pathways whose strength is one or two order of magnitude larger than the rest of pathways. Thus, for m top or bottom samples we count the number of the paths with strength larger than 1000 cm^{-1} as a measure for having a few dominant paths. In Figs. 10(a) and 10(b) we compute the average of this measure for m high and low ETE samples ($m = 10-90, 100-900, 1000-5000$) and for $d = 30, 60, 90 \text{ \AA}$. Remarkably, it can be observed that all of top 500 high efficient samples do not have any number of dominant paths, see Fig. 10(a). However, as we compute the average over a larger number of high efficient samples some stronger paths will emerge. As expected, the inverse behavior is observed for low efficient samples presented in Fig. 10(b), where the low ETE configurations have some dominant pathways that disappear as we increase the number of low ETE samples. These results demonstrate that the path strength, defined by Eq. (10), captures the spatial correlations among top/low ETE structures and thus can provide an underlying geometrical description for the efficiency of light-harvesting complexes.

IX. CONCLUSION AND OUTLOOK

We studied the energy transport capability of random arrangements of chromophores in volumes of various diameters as a function of chromophoric density, reorganization energy, and their interplay. We demonstrated that the chromophoric density plays a major role in determining the performance of few-chromophoric systems embedded in various spherical volumes. We found that for random multichromophoric systems with fixed sizes 30 \AA and 50 \AA , 7 and 14 chromophores are indeed the minimum numbers to achieve a high ETE, similar to those values for FMO¹⁹ and LHCII, respectively. After our original observations of these optimal chromophoric numbers in biological LHC,¹² a similar result has been recently reported.³⁹

We observed significant statistical correlations in the low- and high-end efficient random structures with respect

to average exciton energy gaps and multichromophoric spatial connectivity at the intermediate system-bath couplings. Moreover, we have investigated possible statistical correlations between quantum entanglement and performance of random chromophoric configurations. Specifically, we simulated the dynamics of excitons for many high/low ETE samples and calculated the entanglement measure based on Ref. 40. Our simulations showed no particular pattern from which one can conclude that the presence of quantum entanglement is a significant indicator of efficient energy transport.

There are a number of possible extensions and generalizations to our study that would be of practical relevance for rational design of artificial light-harvesting systems. One possible extension of our study is to repeat these simulations with bath correlation functions other than near classical exponentially decaying function. For that purpose, we can either use the TC2 Eq. (6) or techniques such as path integral⁴¹ or bath renormalization approaches to modeling decoherence dynamics.^{42,43} In the former case, we need to characterize first the range of accuracy of the TC2 equation by comparison with the exact solutions from the approaches in Ref. 41–43. Other important generalizations are to include real geometrical constraints due to the size or shape of each chromophores, and the various effects of solvent or protein environments. An interesting example of how the protein scaffold can influence ETE has recently been evaluated by quantum chemistry calculations.^{13,44} The heterogeneous dielectric environment can modulate the inter-chromophoric electronic couplings such that the energy transfer rate can be changed by a factor of two over continuum dielectric environments of a liquid solution. Thus the protein scaffold can significantly impact energy transport beyond those factors studied in this work, such as the chromophoric concentrations and their spatial and energetic arrangements. A related modification of our study is the adversarial effect of concentration quenching that can significantly reduce the efficiency of energy transport at high concentrations. However, non-random structural design of the protein scaffold can suppress the damaging effect of concentration quenching,^{13,23} while allowing for high chromophoric densities to optimize energy transport efficiency.

Overall, two distinct parameter regimes for efficient energy transport can be observed. Ideally, one can design molecular configurations to reside in the so-called Quantum Goldilocks regime^{12,45} where there is an energy-scale convergence for coherent and incoherent processes leading to optimality and robustness. However, if such regime is practically inaccessible, here we found alternative scenarios for potential optimal material design beyond Goldilocks regime where certain configurations could still have high energy efficiencies, e.g., due to constructive quantum interference effects, but they become very sensitive to defects or environmental fluctuations. These model studies could be useful for design of structured molecular aggregates such as self-assembled dyes on tubular J-aggregates^{46,47} and virus-based templates aggregates,^{37,38,48,49} with potential applications to photovoltaic devices, photosensing, and biological sensing.

ACKNOWLEDGMENTS

We thank A. Ishizaki, M. Sarovar, and K. B. Whaley, for useful discussions. We acknowledge funding from DARPA under the QuBE program, NSF, ENI, ISI, NEC, Lockheed Martin, Intel, and from project IT-PQuantum, as well as from Fundação para a Ciência e a Tecnologia (Portugal), namely, through programme POCTI/POCI/PTDC, and projects SFRH/BPD/71897/2010, PEst-OE/EEI/LA0008/2013 and PTDC/EEA-TEL/103402/2008 QuantPrivTel, partially funded by EU-FEDER, and from the European Union's Seventh Framework Programme (FP7/2007-2013) under Grant Agreement No. 318287.

- ¹V. May and O. Kuhn, *Charge and Energy Transfer Dynamics in Molecular Systems* (Wiley-VCH, Weinheim, 2004).
- ²S. Mukamel, *Principles of Nonlinear Optical Spectroscopy* (Oxford University Press, USA, 1999).
- ³G. S. Engel, T. R. Calhoun, E. L. Read, T. K. Ahn, T. Mancal, Y. C. Cheng, R. E. Blankenship, and G. R. Fleming, *Nature (London)* **446**, 782 (2007).
- ⁴M. Mohseni, P. Rebentrost, S. Lloyd, and A. Aspuru-Guzik, *J. Chem. Phys.* **129**, 174106 (2008).
- ⁵P. Rebentrost, M. Mohseni, and A. Aspuru-Guzik, *J. Phys. Chem. B* **113**, 9942 (2009).
- ⁶P. Rebentrost, M. Mohseni, I. Kassal, S. Lloyd, and A. Aspuru-Guzik, *New J. Phys.* **11**, 033003 (2009).
- ⁷M. B. Plenio and S. F. Huelga, *New J. Phys.* **10**, 113019 (2008).
- ⁸J. Cao and R. Silbey, *J. Phys. Chem. A* **113**, 13825 (2009).
- ⁹F. Caruso, A. W. Chin, A. Datta, S. F. Huelga, and M. B. Plenio, *Phys. Rev. A* **81**, 062346 (2010).
- ¹⁰G. Panitchayangkoon, D. Hayes, K. A. Fransted, J. R. Caram, E. Harel, J. Wen, R. E. Blankenship, and G. S. Engel, *Proc. Natl. Acad. Sci. U.S.A.* **107**, 12766 (2010).
- ¹¹A. Shabani, M. Mohseni, H. Rabitz, and S. Lloyd, *Phys. Rev. E* **86**, 011915 (2012).
- ¹²M. Mohseni, A. Shabani, H. Rabitz, and S. Lloyd, e-print [arXiv:1103.3823](https://arxiv.org/abs/1103.3823).
- ¹³G. D. Scholes, G. R. Fleming, A. Olaya-Castro, and R. V. Grondelle, *Nat. Chem.* **3**, 763 (2011).
- ¹⁴*Quantum Effects in Biology*, edited by M. Mohseni, Y. Omar, G. Engel, and M. Plenio (Cambridge University Press, Cambridge, UK, 2013).
- ¹⁵S. Lloyd and M. Mohseni, *New J. Phys.* **12**, 075020 (2010).
- ¹⁶D. Abasto, M. Mohseni, S. Lloyd, and P. Zanardi, *Philos. Trans. R. Soc. London, Ser. A* **370**, 3750 (2012).
- ¹⁷R. E. Blankenship, *Molecular Mechanism of Photosynthesis* (Blackwell Science, London, 2002).
- ¹⁸H. Lee, Y.-C. Cheng, and G. R. Fleming, *Science* **316**, 1462 (2007).
- ¹⁹Until recently it was believed that the number of chromophores for FMO is seven, but recent studies suggest the existence of an eighth shared chromophore between the FMO three monomers; e.g., please see M. Schmidt am Busch, F. Muh, M. E. A. Madjet, and T. Renger, *J. Phys. Chem. Lett.* **2**, 93 (2011).
- ²⁰T. R. Calhoun, N. S. Ginsberg, G. S. Schlau-Cohen, Y.-C. Cheng, M. Ballottari, R. Bassi, and G. R. Fleming, *J. Phys. Chem. B* **113**, 16291 (2009).
- ²¹T. Scholak, F. D. Melo, T. Wellens, F. Mintert, and A. Buchleitner, *Phys. Rev. E* **83**, 021912 (2011).
- ²²H.-P. Breuer and F. Petruccione, *The Theory of Open Quantum Systems* (Oxford University Press, New York, 2002).
- ²³G. S. Beddard and G. Porter, *Nature (London)* **260**, 366 (1976).
- ²⁴J. Cao, *J. Chem. Phys.* **107**, 3204 (1997).
- ²⁵A. Ishizaki and G. R. Fleming, *J. Chem. Phys.* **130**, 234110 (2009).
- ²⁶T. Ritz, S. Park, and K. Schulten, *J. Phys. Chem. B* **105**, 8259 (2001).
- ²⁷A. Olaya-Castro, C. Fan Lee, F. Fassioli Olsen, and N. F. Johnson, *Phys. Rev. B* **78**, 085115 (2008).
- ²⁸S. Hoyer, M. Sarovar, and K. B. Whaley, *New J. Phys.* **12**, 065041 (2010).
- ²⁹A. Ishizaki and G. R. Fleming, *Proc. Natl. Acad. Sci. U.S.A.* **106**, 17255 (2009).
- ³⁰G. D. Scholes, *Annu. Rev. Phys. Chem.* **54**, 57–87 (2003).

- ³¹In this work, whenever it is not specified otherwise, the environmental parameters for the FMO complex are chosen according to the estimated values of reorganization energy 35 cm^{-1} , bath cutoff frequency 50 cm^{-1} , temperature 298°K , trapping rate of 1 ps , exciton lifetime of 1 ns .
- ³²T. Förster, in *Modern Quantum Chemistry*, Istanbul Lectures, edited by O. Sinanoglu (Academic, New York, 1965), Vol. 3, pp. 93–137.
- ³³M. Yang and G. R. Fleming, *Chem. Phys.* **275**, 355 (2002).
- ³⁴A. Kolli *et al.*, *J. Chem. Phys.* **137**, 174109 (2012).
- ³⁵A. W. Chin *et al.*, *Philos. Trans. R. Soc. London, Ser. A* **370**, 3638–3657 (2012).
- ³⁶A. W. Chin *et al.*, *Nat. Phys.* **9**, 113 (2013).
- ³⁷Y.-Z. Ma, R. A. Miller, G. R. Fleming, and M. B. Francis, *J. Phys. Chem. B* **112**, 6887 (2008).
- ³⁸R. A. Miller, N. Stephanopoulos, J. M. McFarland, A. S. Rosko, P. L. Geissler, and M. B. Francis, *J. Am. Chem. Soc.* **132**, 6068 (2010).
- ³⁹S. Jesenko and M. Znidaric, *New J. Phys.* **14**, 093017 (2012).
- ⁴⁰M. Sarovar, A. Ishizaki, G. R. Fleming, and K. B. Whaley, *Nat. Phys.* **6**, 462 (2010).
- ⁴¹S. Weiss *et al.*, *Phys. Rev. B* **77**, 195316 (2008).
- ⁴²J. Prior *et al.*, *Phys. Rev. Lett.* **105**, 050404 (2010).
- ⁴³A. W. Chin *et al.*, *J. Math. Phys.* **51**, 092109 (2010).
- ⁴⁴C. Curutchet *et al.*, *J. Am. Chem. Soc.* **133**, 3078 (2011).
- ⁴⁵S. Lloyd, M. Mohseni, A. Shabani, and H. Rabitz, e-print [arXiv:1111.4982](https://arxiv.org/abs/1111.4982).
- ⁴⁶D. M. Eisele *et al.*, *Nat. Nanotechnol.* **4**, 658 (2009).
- ⁴⁷D. M. Eisele *et al.*, *Nat. Chem.* **4**, 655 (2012).
- ⁴⁸Y. S. Nam *et al.*, *J. Am. Chem. Soc.* **132**, 1462 (2010).
- ⁴⁹X. Dang *et al.*, *Nat. Nanotechnol.* **6**, 377 (2011).